

# Novel Driving Method For BLDCM From Standstill To High Speeds

Wang Hua-bin, Liu He-ping

State Key Laboratory of Power Transmission Equipment  
& System Security and New Technology

Chongqing University

129-1 Room of 6th Building of College of Electrical Engineering, 400030  
China

E-mail: wanghuabin929@yahoo.cn

*Abstract-* A novel approach is proposed which can drive an interior permanent magnet (IPM) brushless DC motor (BLDCM) smoothly from standstill to high speeds without position or speed sensors. At standstill, initial rotor position is estimated by using the inductance variation due to the magnet position. In rotating condition, indirect inductance method was implemented for BLDCM with H\_PWM-L\_PWM modulation scheme at very low speeds; When the motor speed is beyond a certain speed where the back EMF is enough, the sensorless algorithm for rotor position detection is switched to the back EMF method to drive the IPM BLDCM with H\_PWM-L\_ON modulation scheme. The validity of the proposed method is verified through Experimental results.

*Keywords-* Interior Permanent Magnet , Brushless DC motor, Back EMF method, Indirect Inductance Method, Sensorless

## 1. Introduction

A BLDCM is used in various applications of electromechanical systems because of its high efficiency and good controllability over a wide range of speeds. The drive for the brushless DC motor requires a position sensor for providing proper commutation sequence to turn on the power devices in the inverter bridge. Position sensor not only increases the cost and encumbrance of the overall drive system but also reduces its control robustness and reliability. Furthermore, it might be difficult to install and maintain a position sensor due to the limited assembly space and rigid working environment with severe vibration and/or high temperature. Therefore, Several main techniques of sensorless control of BLDCM have been extensively studied, which can be categorized into the following:

1) Back-EMF Sensing Techniques

These methods include terminal voltage sensing of the motor<sup>[1][2]</sup>; detection of the conducting state of

freewheeling diode in the unexcited phase<sup>[3]</sup>; back-EMF integration method<sup>[4][5]</sup>; Stator third harmonic voltage components<sup>[6]</sup>. These methods have been shown to be successful only at medium and high rotor speeds.

2) Flux Linkage-Based Technique<sup>[7-8]</sup>

In these methods, the flux linkage is calculated using measured voltages and currents. The fundamental idea is to take the voltage equation of the machine and by integrating the applied voltage and current, flux can be estimated. From the initial position, machine parameters, and the flux linkages' relationship to rotor position, the rotor position can be estimated. This method also has significant estimation error in low speeds.

3) Estimators based on inductance variation due to geometrical and saturation effects<sup>[9-15]</sup>:

The rotor position can be estimated by using inductance variations due to magnetic saturation and/or geometrical effects of BLDCM. An

“INFORM” method was proposed by Schroedl, which was based on real-time inductance measurements using saliency and saturation effects. During a short time interval, the “complex INFORM reactance” was calculated for estimating flux angle<sup>[9]</sup>. Corley and Lorenz<sup>[10]</sup> investigated a high frequency signal injection method in such a way that carrier-frequency voltages were applied to the stator windings of PMSM, producing high-frequency currents of which the magnitude varies with rotor position. However, all these methods require high-precision and high-bandwidth (fast) measurement and fast signal processing capability, which inevitably increase the complexity and cost of control system.

4) methods using state observers<sup>[16-21]</sup>:

Lim et al proposed a pair of cascaded Luenberger observers, of which the faster one was for the estimation of rotor position using current measurements and the slower one for estimating angular velocity<sup>[16]</sup>. Kim et al also proposed a Luenberger observer which provided a simple estimation process as a kind of reduced-order state observer to obtain back-EMF information<sup>[17]</sup>.

However, the poles and zeros of system transfer function could vary due to parameter variations, and model uncertainties may degrade the performances of these observers.

5) Extended Kalman filters:

The Extended Kalman Filter (EKF) is able to provide optimum filtering of the noises in measurement and inside the system if the covariances of these noises are known. It is an optimal stochastic observer in the least-square sense for estimating the states of dynamic non-linear systems. Hence it is a viable candidate for the on-line determination of the rotor position and speed<sup>[22-24]</sup>. However, none of the practical industry applications of EKF-based sensorless PMSM control has been reported due to the technical difficulties.

6) Fuzzy-logic, neural network and artificial intelligence-based estimators:

fuzzy-logic, neural network and artificial

intelligence-based estimators have been presented for the sensorless control<sup>[25-27]</sup>. These methods use artificial neural network (ANN), diagonally recurrent neural network or fuzzy-neural network combined with adaptive technique. They are completely different from traditional model-based estimation methods as discussed above.

This paper presents a new drive method which can drive IPM BLDCM smoothly from standstill to high speeds. In full speed range, two sensorless methods were used alternatively. In low speed, we use indirect inductance method; when speed is above a certain speed, sensorless control method will be transferred to the back EMF method.

## 2. Model of Inductance of IPM BLDCM

BLDCM can be categorized into IPM motors and surface mounted permanent magnet (SPM) motors. Compared with SPM motors, IPM motors have a mechanically robust and solid structure since the magnets are physically contained and protected. So IPM motors are more practical than SMP motors in various industrial and other applications. In a BLDCM, the back EMF induced by the rotary PM excitation field is approximately trapezoidal, as shown in Fig.1.

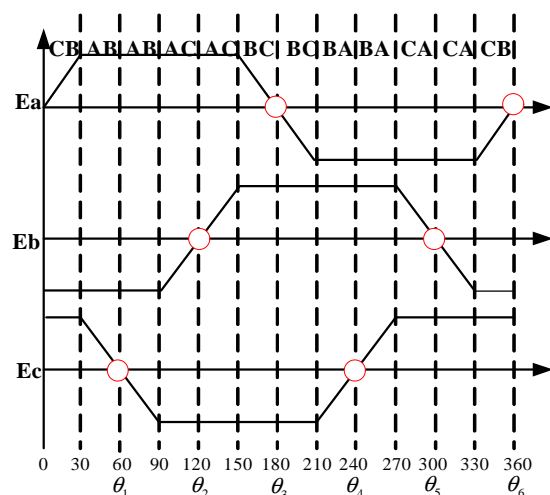


Fig. 1 Ideal back EMF waveforms

The IPM BLDCM is characterized by the fact that its phase inductance varies appreciably as a function of the rotor position. The variation of phase inductance of an IPM motor is similar to that

of a conventional salient pole synchronous motor with one important difference. The conventional wound rotor salient pole synchronous motor has  $I_d > I_q$ . In contrast, In the IPM BLDCM, the air gap in the d axis is small while there is a large air-gap in the q axis. The d axis inductance will in this case be larger than the inductance in the q axis.

Fig.2 shows an idealized IPM motor. It is clear from the Fig.2 that the A-phase self inductance is minimum when the rotor field axis(known as the direct axis) is aligned with the magnetic axis of A-phase and is maximum when the rotor is rotated 90 degree from this position.

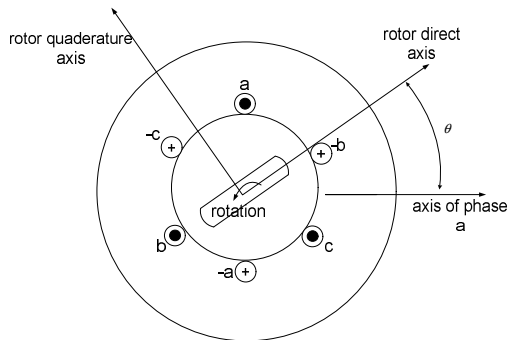


Fig.2 Idealized 3-phase ,2-pole permanent magnet motor(salient pole)

As a salient pole permanent magnet motor<sup>[28][29]</sup>, the winding inductance varies significantly with the rotor position. The stator self inductances of IPM BLDCM can be approximately expressed as

$$\begin{cases} l_{aa} = L_{aa0} + L_{al} + L_{g2} \cos(2\theta) \\ l_{bb} = L_{aa0} + L_{al} + L_{g2} \cos(2\theta + \frac{2\pi}{3}) \\ l_{cc} = L_{aa0} + L_{al} + L_{g2} \cos(2\theta - \frac{2\pi}{3}) \end{cases} \quad (1)$$

The stator-to-stator mutual inductances are

$$\begin{cases} l_{ab} = l_{ba} = -0.5L_{aa0} + L_{g2} \cos(2\theta - \frac{2\pi}{3}) \\ l_{bc} = l_{cb} = -0.5L_{aa0} + L_{g2} \cos(2\theta) \\ l_{ac} = l_{ca} = -0.5L_{aa0} + L_{g2} \cos(2\theta + \frac{2\pi}{3}) \end{cases} \quad (2)$$

Where

$\theta$  Electrical rotor angle

$L_{aa0}$  Component of the self inductance due to the space fundamental air-gap flux

$L_{al}$  Additional component due to the armature leakage flux

$L_{g2}$  Component of the self inductance due to rotor position dependent flux

Table.1 Relationship among rotor position, back EMF, self inductance, mutual inductance

Rotor position	Self inductance	back EMF		Mutual inductance
$\theta = 60^\circ$	$l_{aa} = l_{bb}$	$E_a = -E_b$	$E_c = 0$	$l_{bc} = l_{ac}$
$\theta = 120^\circ$	$l_{aa} = l_{cc}$	$E_a = -E_c$	$E_b = 0$	$l_{ab} = l_{bc}$
$\theta = 180^\circ$	$l_{cc} = l_{bb}$	$E_b = -E_c$	$E_a = 0$	$l_{ab} = l_{ac}$
$\theta = 240^\circ$	$l_{aa} = l_{bb}$	$E_a = -E_b$	$E_b = 0$	$l_{bc} = l_{ac}$
$\theta = 300^\circ$	$l_{aa} = l_{cc}$	$E_a = -E_c$	$E_c = 0$	$l_{ab} = l_{bc}$
$\theta = 360^\circ$	$l_{cc} = l_{bb}$	$E_b = -E_c$	$E_a = 0$	$l_{ab} = l_{ac}$

It is well known that the zero-cross point(ZCP) of the back EMF of a particular phase occurs 30 electrical degrees before that phase is energized. But the ZCP of a phase winding also coincides with alignment of the magnetic axis of that winding with the d-axis of the rotor. Clearly at that position, the self inductance of that phase is a maximum, whereas the inductances of the two other phases will, because of geometric symmetry, be equal to each other. In other words, wherever the rotor d axis aligns with the magnetic axis of the A-phase winding,  $E_a$  is equal to zero and  $l_{bb} = l_{cc}$ . Similar statements can be made about the B-phase winding and the C-phase winding. Therefore the positions of equal inductance of the energized phases, just like the ZCP of the back EMF of the floating phase occur 30 electrical degrees before the next commutation position. Table.1 gives exact relationships among rotor positions and self-inductances or mutual inductances or back EMF. It is shown that the rotor position where the self inductance is equal coincides

with the ZCP of back EMF of the unenergized phase according to Table.1. Therefore, some methods which can detect the equal inductance of energized phases in real time can be used for the commutation of BLDCM.

### 3 The Analyse of New Drive Method For IPM BLDCM

#### 3.1 The principle of the indirect inductance method

It is well known that the back EMF sensing techniques fail at very low speeds, so a new method, indirect inductance method for sensorless control, is proposed to solve the problem. The method is also based on the fact that the phase inductance of IPM machine varies with the rotor position. But it does not measure phase inductance directly, but detects whether the self inductance of energized phases is equal or not, which is different from the conventional sensorless methods based inductance variations.

As three phase inverter is concerned, PWM control scheme<sup>[30]</sup> is widely applied to control the speed and current of BLDCM. The PWM scheme that is used in this paper is H\_PWM-L\_PWM. Fig.3 illustrates the gating sequence of the electronic switches waveforms in this typical PWM strategy in which both the active switches in the lower half bridge and upper half bridge are modulated simultaneously.

The selected interval for subsequent analysis shown in Fig.4 corresponds to instant when the current is beginning to switch from A-phase into B-phase whereas the current of C-phase is assumed to have already decayed to zero. During the interval switches  $T_A^+$  and  $T_B^-$  are only two active switches. When the switches  $T_A^+$  and  $T_B^-$  are switched off shown in Fig.5, the phase current is circulating through freewheeling diodes  $D_B^+$  and  $D_A^-$ . The dashed line in Fig.4 and Fig.5 illustrates the real loop current direction.

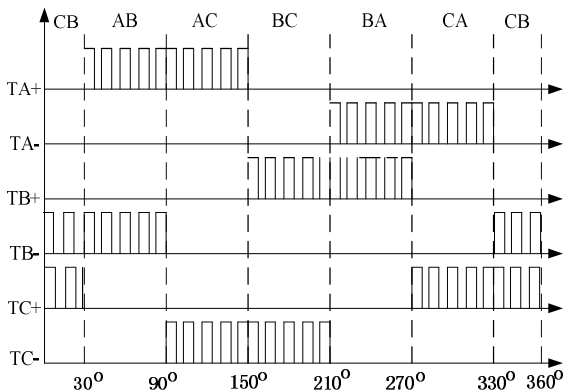


Fig.3 Timing diagram of H\_PWM-L\_PWM control signals

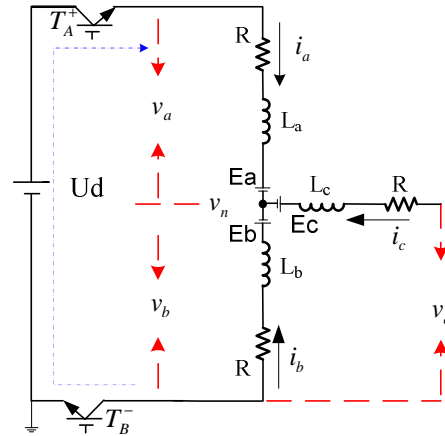


Fig.4 equivalent circuit during the switch-on When C-phase is open

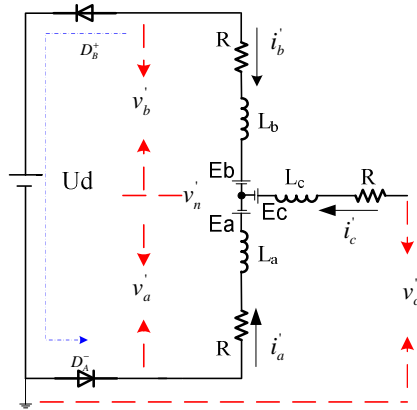


Fig.5 equivalent circuit during the switch-off When C-phase is open

The circuit equations of Fig.4 are

$$\begin{cases} v_a = l_{aa} \frac{di_a}{dt} + i_a \frac{dl_{aa}}{dt} + l_{ab} \frac{di_b}{dt} + i_b \frac{dl_{ab}}{dt} + i_a R + E_a \\ v_b = l_{ab} \frac{di_a}{dt} + i_a \frac{dl_{ab}}{dt} + l_{bb} \frac{di_b}{dt} + i_b \frac{dl_{bb}}{dt} + i_b R + E_b \\ v_c = l_{ac} \frac{di_a}{dt} + l_{bc} \frac{di_b}{dt} + i_a \frac{dl_{ac}}{dt} + i_b \frac{dl_{bc}}{dt} + E_c + v_n \\ i_a = -i_b, i_c = 0 \end{cases} \quad (3)$$

$$U_d = v_a - v_b + 2V_s \quad (4)$$

$$v_n = -v_b + V_s \quad (5)$$

Where  $V_s$  is the inverter switch on-state voltage drop.

Substituting (4) and (5) into (3) gives

$$\begin{cases} v_n = \frac{U_d}{2} + \frac{(l_{bb} - l_{aa})}{2} \frac{di_a}{dt} + \frac{i_a}{2} \frac{d(l_{bb} - l_{aa})}{dt} - \frac{(E_a + E_b)}{2} \\ v_c = v_n + (l_{ac} - l_{bc}) \frac{di_a}{dt} + i_a \frac{d(l_{ac} - l_{bc})}{dt} + E_c \end{cases} \quad (6)$$

If back EMF is assumed constant in the PWM

cycle. From Table.1, it is found  $l_{aa}$  is equal to  $l_{bb}$ ,  $E_a$  is equal to  $-E_b$ ,  $l_{bc}$  is equal to  $l_{ac}$  where  $\theta$  is at  $60^\circ$  or  $240^\circ$ . So the potential of C phase is

$$v_c = \frac{U_d}{2} + E_c \quad \theta = 60^\circ \text{ or } 240^\circ \quad (7)$$

The circuit equations of Fig.5 are

$$\begin{cases} v_a' = l_{aa} \frac{di_a'}{dt} + i_a' \frac{dl_{aa}}{dt} + l_{ab} \frac{di_b'}{dt} + i_b' \frac{dl_{ab}}{dt} + i_a' R + E_a \\ v_b' = l_{ab} \frac{di_a'}{dt} + i_a' \frac{dl_{ab}}{dt} + l_{bb} \frac{di_b'}{dt} + i_b' \frac{dl_{bb}}{dt} + i_b' R + E_b \\ v_c' = l_{ac} \frac{di_a'}{dt} + l_{bc} \frac{di_b'}{dt} + i_a' \frac{dl_{ac}}{dt} + i_b' \frac{dl_{bc}}{dt} + E_c + v_n' \\ i_a' = -i_b', i_c' = 0 \end{cases} \quad (8)$$

$$U_d = v_b' - v_a' - 2V_D \quad (9)$$

$$v_n = -v_a - V_D \quad (10)$$

Where  $V_D$  is the inverter diode on-state voltage drop. Substituting (9) and (10) into (8) gives

$$\begin{cases} v_n' = \frac{U_d}{2} + \frac{(l_{bb} - l_{aa})}{2} \frac{di_a'}{dt} + \frac{i_a'}{2} \frac{d(l_{bb} - l_{aa})}{dt} - \frac{(E_a + E_b)}{2} \\ v_c' = v_n' + (l_{ac} - l_{bc}) \frac{di_a'}{dt} + i_a' \frac{d(l_{ac} - l_{bc})}{dt} + E_c \end{cases} \quad (11)$$

When  $\theta$  is at  $60^\circ$  or  $240^\circ$ , with Table.1, the potential of C-phase,  $v_c'$ , can be represented as

$$v_c' = \frac{U_d}{2} + E_c \quad \theta = 60^\circ \text{ or } 240^\circ \quad (12)$$

Comparing (7) with (12) gives

$$\Delta v_c = v_c - v_c' = 0 \quad \theta = 60^\circ \text{ or } 240^\circ \quad (13)$$

Analyzing Table.1, it is known that  $E_c$  is equal to zero when  $\theta$  is equal to  $60^\circ$  or  $240^\circ$ . Therefore, the ZCP of back EMF of C-phase can be estimated by computing the differences of terminal voltage of C-phase according to (13). Simultaneously, we can get the equivalent Circuit shown in Fig.6-Fig.9 when B-phase or A-phase is open with H\_PWM-L\_PWM modulation scheme.

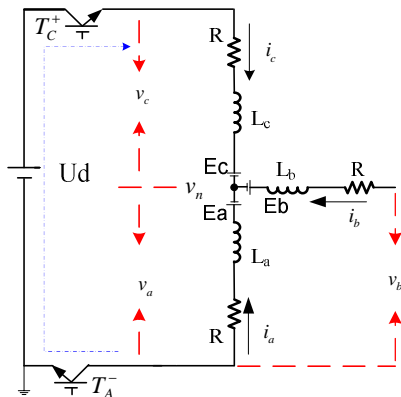


Fig.6 equivalent circuit during the switch-off When B-phase is open

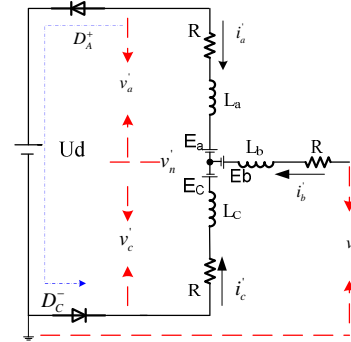


Fig.7 equivalent circuit during the switch-off When B-phase is open

Similarly, According to Fig.6 and Fig.7, when  $\theta$  is at  $180^\circ$  or  $360^\circ$ , the potential of A-phase,  $v_a$  and

$v_a'$ , can be represented as

$$v_a = \frac{U_d}{2} + E_a, \quad v_a' = \frac{U_d}{2} + E_a \quad (14)$$

$$\Delta v_a = v_a - v_a' = 0 \quad \theta = 180^\circ \text{ or } 360^\circ \quad (15)$$

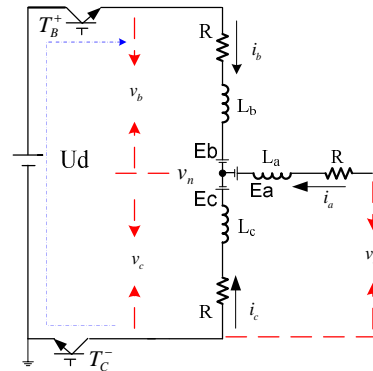


Fig.8 equivalent circuit during the switch-on When A-phase is open

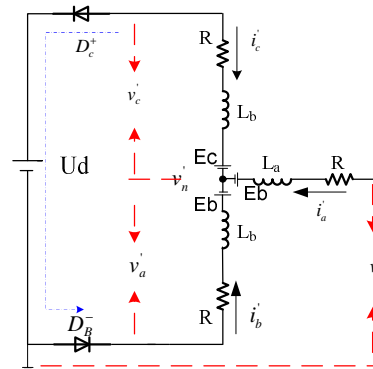


Fig.9 equivalent circuit during the switch-off When A-phase is open

According to the Fig.8 and Fig.9, When  $\theta$  is at  $120^\circ$  or  $300^\circ$ , the potential of B phase,  $v_b$  and

$v'_b$ , can be represented as

$$v_b = \frac{U_d}{2} + E_b, v'_b = \frac{U_d}{2} + E_b \quad (16)$$

$$\Delta v_b = v_b - v'_b = 0 \quad \theta = 120^\circ \text{ or } 300^\circ \quad (17)$$

### 3.2 Analysis of the sensitivity of indirect inductance method

When rotor position is at any position and under the assumption that the current of C-phase have decayed to zero, A-phase and B-phase are modulated simultaneously shown in Fig.4, Fig.5 and Fig.6 in which T is the PWM period and t is the switch on-state time show the A-phase current waveform in a H\_PWM-L\_PWM cycle.

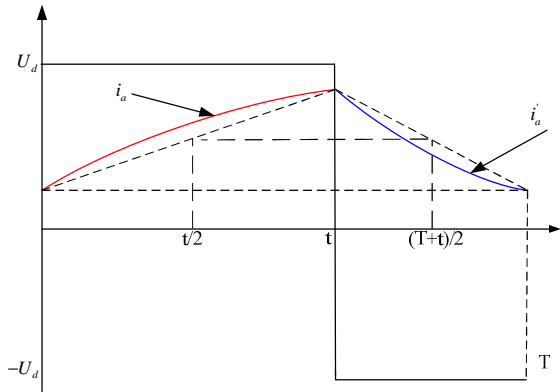


Fig.10 the phase current waveform in a PWM period

According to Fig.4, Combining (3) and (4) or (5) can give

$$\frac{di_a}{dt} = \frac{\left( \frac{U_d - i_a}{2} \frac{d\left(\frac{l_{aa} + l_{bb} - l_{ab}}{2}\right)}{dt} - \frac{E_a - E_b - V_s - i_a R}{2} \right)}{\left(\frac{l_{aa} + l_{bb} - l_{ab}}{2}\right)} \quad (18)$$

According to Fig.5, Combining (8) and (9) or (10) can give

$$\frac{di'_a}{dt} = \frac{\left( \frac{U_d + i'_a}{2} \frac{d\left(\frac{l_{aa} + l_{bb} - l_{ab}}{2}\right)}{dt} + \frac{E_a - E_b + V_D + i'_a R}{2} \right)}{\left(\frac{l_{aa} + l_{bb} - l_{ab}}{2}\right)} \quad (19)$$

According to similar triangle principle, Fig.10 can give approximately

$$i_a(t/2) = i'_a((t+T)/2) \quad (20)$$

The voltage difference between  $v_c(t/2)$  and  $v'_c((t+T)/2)$ ,  $\Delta v_c(T)$ , can be represented as

$$\Delta v_c(T) = v_c(t/2) - v'_c((t+T)/2) \quad (21)$$

Substituting (3), (8), (18), (19), (20) into (21) gives

$$\Delta v_c(T) = \left\{ (l_{ac} - l_{bc}) + \left(\frac{l_{bb} - l_{aa}}{2}\right) \right\} \left( \frac{U_d - V_s + V_D}{\frac{l_{aa} + l_{bb} - l_{ab}}{2}} \right) \quad (22)$$

According to (1) and (2), we have

$$\begin{cases} \left(\frac{l_{bb} - l_{aa}}{2}\right) = \frac{\sqrt{3}}{2} L_{g2} \cos(2\theta + \frac{5\pi}{6}) \\ l_{ac} - l_{bc} = \sqrt{3} L_{g2} \cos(2\theta + \frac{5\pi}{6}) \end{cases} \quad (23)$$

If the difference of  $V_s - V_D$  is ignored, substituting (23) into (22) gives

$$\Delta v_c(T) = \frac{U_d \left( \frac{3\sqrt{3}}{2} L_{g2} \cos(2\theta + \frac{5\pi}{6}) \right)}{\frac{l_{aa} + l_{bb} - l_{ab}}{2}} \quad (24)$$

The direct and the quadrature axis inductance are

$$\begin{cases} L_d = L_{al} + \frac{3}{2}(L_{aa0} + L_{g2}) \\ L_q = L_{al} + \frac{3}{2}(L_{aa0} - L_{g2}) \end{cases} \quad (25)$$

$$\frac{L_d + L_q}{2} = L_{al} + 1.5L_{aa0} \quad (26)$$

$$\frac{l_{aa} + l_{bb} - l_{ab}}{2} = L_{al} + 1.5L_{aa0} +$$

$$L_{g2} \left( \frac{\cos 2\theta + \cos(2\theta + \frac{2\pi}{3})}{2} - \cos 2\theta \right) \quad (27)$$

It is assumed that the IPM BLDCM has low saliency ratio. Therefore, comparing (25) with (27) and neglecting the last term of (27), we obtain approximately

$$\frac{L_d + L_q}{2} = \frac{l_{aa} + l_{bb} - l_{ab}}{2} \quad (28)$$

Substituting (28) into (24) gives

$$\Delta v_c(T) = \frac{U_d \left( \frac{3\sqrt{3}}{2} L_{g2} \cos(2\theta + \frac{5\pi}{6}) \right)}{\frac{L_d + L_q}{2}} \quad (29)$$

Similarly, with analyzing Fig.6 and Fig.7, we have

$$\Delta v_a(T) = \frac{U_d \left( \frac{3\sqrt{3}}{2} L_{g2} \cos(2\theta + \frac{3\pi}{2}) \right)}{\frac{L_d + L_q}{2}} \quad (30)$$

Also, with analyzing Fig.8 and Fig.9, we have

$$\Delta v_b(T) = \frac{U_d \left( \frac{3\sqrt{3}}{2} L_{g2} \cos(2\theta + \frac{\pi}{6}) \right)}{\frac{L_d + L_q}{2}} \quad (31)$$

According to (29), (30), (31), we can know that the differences ( $\Delta v_a, \Delta v_b, \Delta v_c$ ) depend only on quadrature inductance  $L_q$ , direct inductance  $L_d$  and dc link bus voltage, which are constant in the circuit. Therefore, the indirect inductance method is robust to the speed of BLDCM. Theoretically, it can operate at any low speeds even zero speed.

**3.3 Transfer to or from the back EMF method**

It may be advantageous in applications that the sensorless algorithm is transferred to the back EMF method with H\_PWM-L\_ON modulation scheme above a certain rotor speed, because there are more switching losses in H\_PWM-L\_PWM modulation scheme.

The back EMF method of commutation control relies on detection of the ZCP of the back EMF signal from the unenergized phase. It has been shown that the instant at which the rotor reaches the equal self inductance position coincides with the ZCP of the back EMF of the unenergized phase. There is, therefore, a close parallel between the indirect inductance method and the back EMF method. The close parallel between the two methods makes it easy to implement changeover strategies from one to the other as the motor speed crosses the chosen boundary between low speed and high speed operation.

A transfer scheme is suggested in Fig.11. The transfer scheme includes hysteresis to avoid instability near the transition speed. At speeds lower than  $H^-$  (Fig.11), the indirect inductance method is used. At speeds higher than  $H^+$ , the back EMF method is used. Usually, the back EMF is high enough when the rotor speed is above 25% rated speed, so it can be reference value of the  $H^+$  and  $H^-$ .

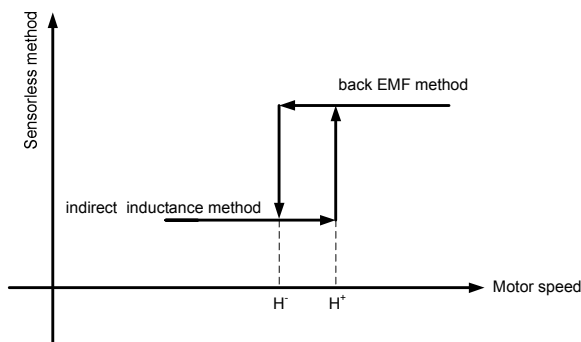


Fig.11 The switch of two sensorless methods

**4 Initial Rotor Position Estimation Method**

At standstill, the motor currents and voltages are zero, so the system of rotor position estimation gives no information for the initial position.

Therefore, another technique has to be found for rotor position estimation at standstill so as to achieve a stable start. The only information that one can use is based on the inductance of phase that is a function of the rotor position due to saliencies of the IPM BLDCM. This approach does not depend on any motor specific characteristics. This method relies on the fact that if voltage is applied across an inductor which is in the presence of a permanent magnet, the resulting current will either add or subtract to the external field created by the permanent magnet, which leads to a further decrease or increase in the inductance. In the case of a BLDCM, the inductor is the stator while the permanent magnet is the rotor.

The implementation of this method requires that a voltage is applied for a fixed time such that it creates a magnetic field in the direction of only one winding. Two magnetic fields of opposite directions should be created for each winding. In order to do this, two phases are held to ground and one is switched to high, creating the forward magnetic field. Then two are switched to high and one is held to ground, creating the opposing magnetic field. This procedure is shown in Fig.12 where phase A is energized in the forward direction.

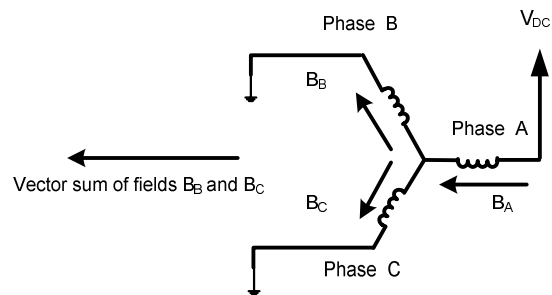


Fig .12 Vector sum of fields  $B_A, B_B, B_C$

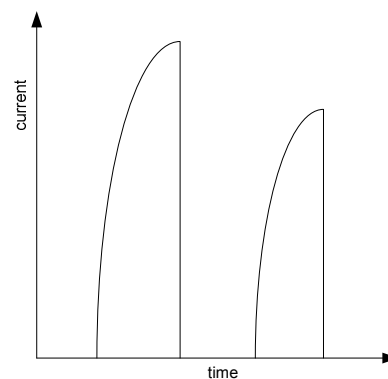


Fig.13 Current pulses

The two peak currents created from the two opposing magnetic fields are then measured and compared. The larger peak will indicate the current

that is in the same direction as the magnetic field caused by the permanent magnet (rotor). Therefore, the polarity of the permanent magnet can be obtained, Figure 13 shows the current peaks produced when the procedure was done with A-phase, given that the rotor is in the position shown in Figure 14. The first current peak which is generated from the forward magnetic field is higher than the one generated from the reverse direction. This means that the magnetic field in the forward direction is in the same direction as that of the magnetic field of the rotor. Thus, the north pole of the rotor is known within 180 degrees.

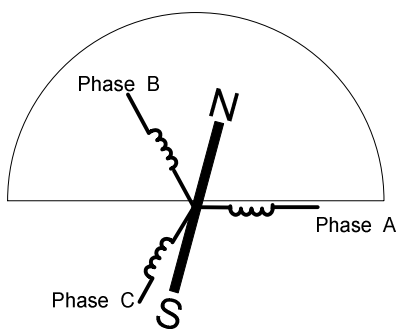


Fig.14 Rotor position 180°

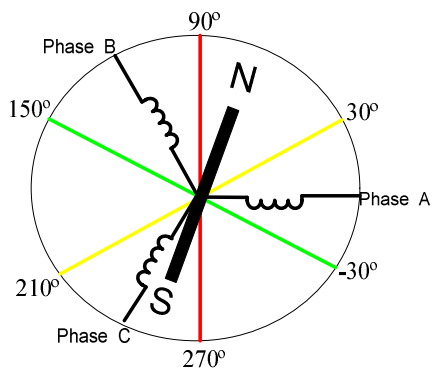


Fig.15 Rotor position 60°

**Table.2 Look-up table for detection of initial rotor position**

Rotor angle	Position code	State to energize
-30° to 30°	100	State 2
30° to 90°	110	State 3
90° to 150°	010	State 4
150° to 210°	011	State 5
210° to 270°	001	State 6
270° to 330°	101	State 1

By repeating the entire procedure for the other two phases, the rotor position can be narrowed down to

within 60 degrees, which is sufficient enough for proper commutation (Fig.15).

To get general regulation, we can list the Table.2. By comparing the pairs of peaks, and assigning a 1 (one) if the first peak is greater, and a 0 (zero) if the second peak is greater will result in a 3 bit binary code. Therefore, we can uniquely determine the initial rotor position with the Table.2.

### 5 Experimental Results

In order to validate the claims made in the proposed approach, the targeted experimental setup was used to implement the proposed method.

Fig.16 shows the prototype of the proposed drive circuit and the adopted IPM machine (5poles, rated power -3KW, and rated speed -2600RPM).The entire drive system is controlled by a cost effective 16 bit micro-controller, Microchip dsPIC6010. The power stage consists of a intelligent power module(750V/60A), which can be directly interfaced with the micro-controller. Fig.17 is the experimental test-bed for BLDCM drives that is built in the State Key Laboratory of Power Transmission Equipment & System Security and New Technology of Chongqing University.

Fig.18 shows 6 current responses when the rotor is at standstill. With the Table.2, we can infer that the initial rotor position is between 210° and 270°

In the Fig.19, experimental results show the real A-phase current waveform and corresponding to the PWM waveform.The experimental waveform of A-phase shows a good agreement with the waveform of theoretical analysis shown in Fig.10.

Fig.20 shows the waveform of three phase terminal voltage with H\_PWM-L\_PWM modulation and commutation signal obtained with indirect inductance method, in which the motor speeds is 58RPM, less than 3% rated speed.

When speed is above 25% rated speed, sensorless control method will transferred to the back EMF method. Fig.21 from top to bottom show the terminal voltage for A-phase and B-phase, C-phase with H\_PWM-L\_ON modulation scheme, obtained the commutation signal using conventional back EMF method, in which the motor speed is 800RPM, higher

than 25% rated speed.

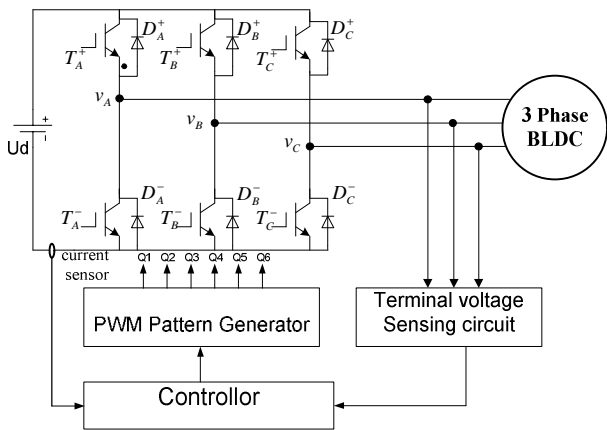


Fig.16 Block diagram of the proposed drive method

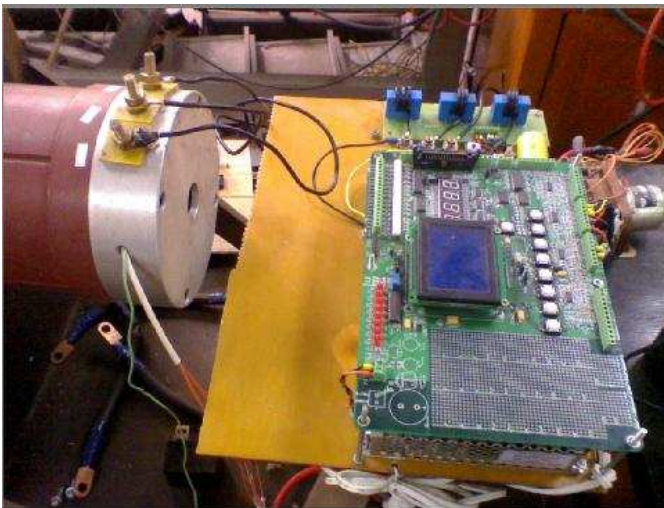


Fig.17 the experimental test-bed for BLDCM drives

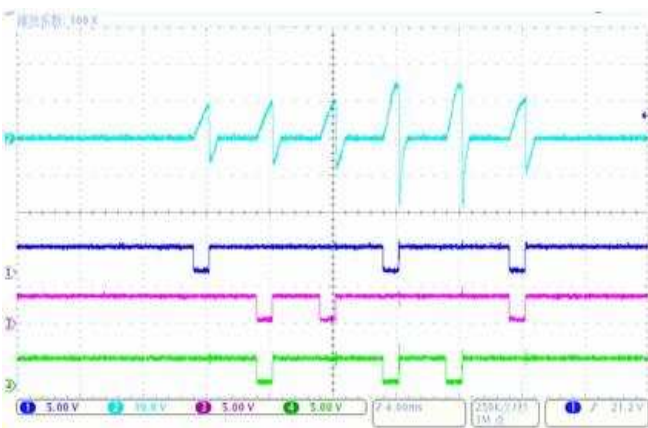


Fig.18 Measured 6 current responses for a stationary rotor

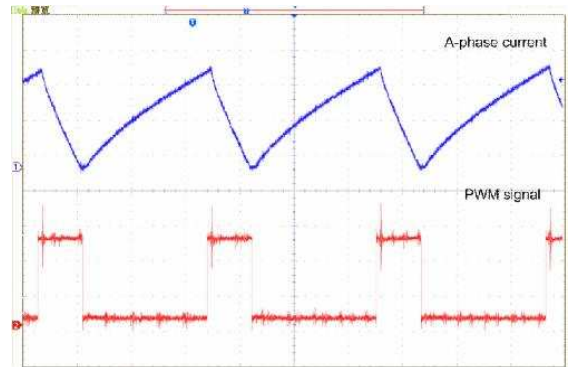


Fig.19 The real A-phase current waveform and corresponded PWM waveform

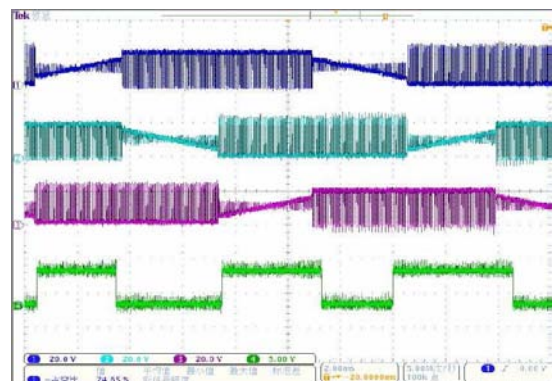


Fig.20 A and B, C phase terminal voltages with H\_PWM-L\_PWM modulation scheme and the commutation signal from indirect inductance method

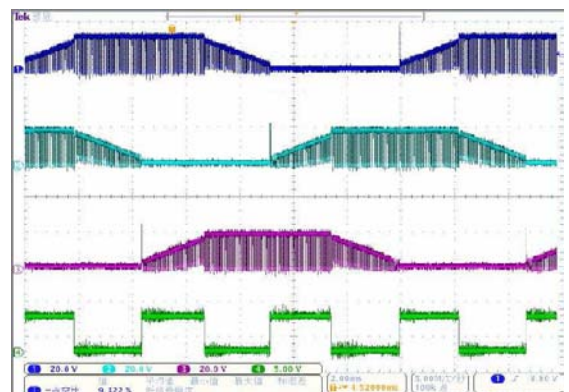


Fig.21 A and B, C phase terminal voltages with H\_PWM-L\_ON modulation scheme and the commutation signal from back EMF method

## 6 Conclusion

This paper presented a novel drive approach for BLDCM which makes it possible to detect the rotor

position over a wide speed range from standstill to high speeds. The estimation of the initial rotor position is based on the investigation of the magnetic saliency without requiring knowledge the motor parameters. In rotating condition, speed and rotor position estimation of BLDCM drive are obtained through two sensorless methods alternatively. The proposed algorithm was implemented in a digital controller using a dsPIC6010 and an experimental speed control system consisting of a BLDCM and a voltage source PWM inverter. The experimental results show that the proposed method has good sensorless speed control performance with initial rotor position estimation. As a result, good controllability over the wide speed range was confirmed, which proved the feasibility of the proposed method.

#### References

- [1] K.Lizuka, H.Uzhashi, M.Kano, T.Endo, and K.Morhri. "Microcomputer Control for Sensorless Brushless Motor". IEEE Transactions on Industry Applications, vol. IA-27, pp. 595-601, 1985.
- [2] J.Shao, D.Nolan, M.Teissier, and D.Swanson. "A Novel Microcontroller-Based Sensorless Brushless DC (BLDC) Motor Drive for Automotive Fuel Pumps". IEEE Transactions on Industry Applications, vol. 39, pp.1734-1740, 2003.
- [3] S.Ogasawara and H.Akagi. "An approach to position Sensorless Drive for Brushless DC Motors". IEEE Transactions on Industry Applications, vol. 27, pp. 928-933, 1991.
- [4] R.C.Becerra, T.M.Jahns, and M.Ehsani. "Four-quadrant sensorless brush-less ECM drive". Applied Power Electronics Conference and Exposition, APEC '91, pp. 202-209, 1991.
- [5] G.-J.Su and J.W.McKeever. "Low Cost Sensorless Control of Brushless DC Motors With Improved Speed Range". IEEE Transactions on Power Electronics, vol. 19, pp. 296-302, 2004.
- [6] J.C.Moreira. "Indirect Sensing for Rotor Flux Position of Permanent Mag net AC Motors Operating in a Wide Speed Range". IEEE Transactions on industry Applications, vol.32,pp.401-407,1996.
- [7] R. Wu and G. R. Slemon. "A permanent magnet motor drive without a shaft sensor". IEEE Trans. Ind. Applicat., vol. 27, pp. 1005-1011, Sept./Oct. 1991.
- [8] S. Ogasawara and H. Akagi. "An approach to position sensorless drive for brushless dc motors". IEEE Trans. Ind. Applicat., vol. 27, pp. 928-933, Sept./Oct. 1991.
- [9] M. Schroedl. "Sensorless control of AC machines at low speed and standatill based on the "INFORM" method". in Conf. Rec. IEEE-IAS Annu. Meeting, vol. 1, 1996, pp. 270-277.
- [10] M. J. Corley and R. D. Lorenz. "Rotor position and velocity estimation for permanent magnet synchronous machine at standstill and high speed". in Conf. Rec.IEEE-IAS Annu. Meeting, vol. 1, 1996, pp. 36-41.
- [11] R. Mizutani, T. Takeshita and N. Matsui. "Current model-based sensorless drives of salient-pole PMSM at low speed and standstill". IEEE Trans. Ind. Applicat., vol. 34, pp. 841-846, July/August, 1998.
- [12] A. Consoli, G. Scarcella and A. Testa. "Industry application of zero-speed sensorless control techniques for PM synchronous motors". IEEE Trans. Ind. Applicat., vol. 37, pp. 513-521, March/April, 2001.
- [13] M. Tursini, R. Petrella and F. Parasiliti. "Initial rotor position estimation method for PM motors". IEEE Trans. Ind. Applicat., vol. 39, pp. 1630-1640, Nov./Dec., 2003.
- [14] J. Jang, S. Sul, J. Ha and et al. "Sensorless drive of surface-mounted permanentmagnet motor by high-frequency signal injection based on magnetic saliency". IEEE Trans. Ind. Applicat., vol. 39, pp. 1031-1039, July/August, 2003.

- [15] J. Jang, J. Ha and A. Testa. "Analysis of permanent-magnet machine for sensorless control based on high-frequency signal injection". *IEEE Trans. Ind. Applicat.*, vol. 40, pp. 1595-1603, Nov./Dec., 2004.
- [16] K. W. Lim, K. S. Low and M. F. Rahman. "A position observer for permanent magnet synchronous motor drive". *IECON Annu. ConferenceRecord*, pp. 1004-1008, 1994.
- [17] J. S. Kim and S. K. Sul. "High performance PMSM drives without rotational position sensors using reduced order observer". in *Proc. Conf. IEEE IAS Annu. Meeting*, 1995, pp. 75-82.
- [18] J. Kim and S. Sul. "New approach for high-performance PMSM drives without rotational position sensors". *IEEE Trans. Power Electron.*, vol. 12, pp. 904-911, Sept. 1997.
- [19] G. Zhu, A. Kaddouri, and et al. "Nonlinear state observer for the sensorless control of a permanent-magnet AC machine". *IEEE Trans. Ind. Electron.*, vol. 48, pp. 1098-1108, Dec. 2001.
- [20] Y. Yamamoto, Y. Yoshida and T. Ashikaga. "Sensorless control of PM motor using full order flux observer". *IEEJ Trans. Ind. Applt.*, vol. 124, pp. 743-749, Aug. 2004.
- [21] S. Shinnaka. "New "D-state-observer"-based vector control for sensorless drive of permanent-magnet synchronous motors". *IEEE Trans. Ind. Applicat.*, vol. 41, pp. 825-833, May./June. 2005.
- [22] R. Dhaouadi, N. Mohan, and L. Norum. "Design and implementation of an extended Kalman filter for the state estimation of a permanent magnet synchronous motor". *IEEE Trans. Power Electron.*, vol. 6, pp. 491-497, July 1991.
- [23] S. Bolognani, R. Oboe, and M. Ziglitto. "Sensorless full-digital PMSM drive with EKF estimation of speed and rotor position". *IEEE Trans. Ind. Electron.*, vol. 46, pp. 184-191, Feb. 1999.
- [24] A. Qiu and B. Wu. "Sensorless control of permanent magnet synchronous motor using extended Kalman filter". in *Proc. Conf. Of CCECE 2004, Niagara Falls*, pp. 1557-1562.
- [25] I. C. Baik, K. H. Kim, and M. J. Youn. "Robust nonlinear speed control of PM synchronous motor using adaptive and sliding mode control techniques". *Proc. IEE-Elect. Power Applicat.*, vol. 145, no. 4, pp. 369-376, 1998.
- [26] D. Schroöder, C. Schäffner, and U. Lenz. "Neural-net based observers for sensorless drives". in *Proc. 20th Int. Conf. Industrial Electronics Control and Instrumentation (IECON'94)*, vol. 3, Bologna, Italy, 1994, pp. 1599-1610.
- [27] Y. Yi, D. M. Vilathgamuwa, and M. A. Rahman. "Implementation of an artificial neural network based real-time adaptive controller for an interior permanentmagnet motor drive". *IEEE Trans. Ind. Appl.*, vol. 39, no. 1, pp. 96-104, Jan./Feb. 2003.
- [28] J.X.Shen, Tseng KJ. Analyses and compensation of rotor position detection error in sensorless PM brushless DC motordrives[J]. *IEEE Transactions on Energy Conversion*, 2003,18(1):87-93.
- [29] A.Kulkarni,M.Ehsani. A Novel Position Sensor Elimination Technique for the Interior Permanent Magnet Synchronous Motor Drive.*IEEE Trans.on Industry Application*, vol.28, 144-150. Jan/Feb, 1992
- [30] Pinghua Tang ,Tiecai Li. "Common-grounded BLDCM Drive System Based on FPGA". 2007 IEEE International Conference on Automation and Logistics Jinan, China. 18-21 Aug. 2007.pp: 3050-3054.